Frustrated Antiferromagnets with Entanglement Renormalization: Ground State of the Spin-$\frac{1}{2}$ Heisenberg Model on a Kagome Lattice

G. Evenbly and G. Vidal

School of Mathematics and Physics, the University of Queensland, Brisbane 4072, Australia

(Received 23 April 2009; revised manuscript received 10 December 2009; published 7 May 2010)

Entanglement renormalization techniques are applied to numerically investigate the ground state of the spin-$\frac{1}{2}$ Heisenberg model on a kagome lattice. Lattices of $N = \{36, 144, \infty\}$ sites with periodic boundary conditions are considered. For the infinite lattice, the best approximation to the ground state is found to be a valence bond crystal with a 36-site unit cell, compatible with a previous proposal. Its energy per site, $E = -0.432\,21$, is an exact upper bound and is lower than the energy of any previous (gapped or algebraic) spin liquid candidate for the ground state.

DOI: 10.1103/PhysRevLett.104.187203 PACS numbers: 75.10.Jm, 02.70.−c, 03.67.Mn, 05.30.−d

Low dimensional spin-$\frac{1}{2}$ quantum systems have long been the focus of intense research efforts, largely fueled by the search for exotic states of matter. An important example of a geometrically frustrated quantum antiferromagnet [1] is the spin-$\frac{1}{2}$ kagome-lattice Heisenberg model (KLHM). Despite a long history of study, the nature of its ground state remains an open question. Leading proposals include valence bond crystal (VBC) [2–7] and spin liquid (SL) [8–16] ground states. Interest has been further stimulated by recent experimental work on herbertsmithite $ZnCu_3(OH)_6Cl_2$, a possible physical realization of the model [17].

Progress in our understanding of the KLHM has been hindered, as with many other models of frustrated antiferromagnets, by the inapplicability of quantum Monte Carlo methods due to the negative sign problem. Nevertheless, systems with up to 36 sites have been addressed with exact diagonalization [9,18], whereas the density matrix renormalization group (DMRG) has been used to explore lattices of order $N \approx 100$ sites [16]. Unfortunately, it is very difficult to infer the nature of the ground state of an infinite system from these results. The reason is that these lattices are still relatively small given the 36-site unit cell of the leading VBC proposal, or the algebraic decay of correlations in some SL proposals. In larger systems, support for a SL ground state has also been obtained with a SL ansatz [13–15], whereas evidence for a VBC has been obtained for an infinite lattice with a series expansion around an arbitrary dimer covering [6,7], but both approaches are clearly biased.

In this Letter we report new, independent numerical evidence in favor of a VBC ground state for the KLHM model. This is done with entanglement renormalization [19–25], a real space RG approach that, through the proper removal of short-range entanglement, is capable of providing an approximation to ground states of large 2D lattices [24] by means of the multiscale entanglement renormalization ansatz (MERA) [20]. After describing a scheme for the kagome lattice with periodic boundary conditions, we address lattices of $N = \{36, 144, \infty\}$ sites. Our simulations converge to a VBC state compatible with that first proposed by Marston and Zeng [2] and revisited by Nikolic and Senthil [4], and by Singh and Huse [6,7]. For an infinite lattice we obtain an energy per site $E = -0.432\,21$. This energy corresponds to an explicit (MERA) wave function and therefore provides us with a strict upper bound for the true ground state energy. Importantly, its value is lower than the energy of any existing SL ansatz on a sufficiently large lattice, which we interpret as strong evidence for a VBC ground state in the thermodynamic limit. Our results are also the first demonstration of the utility of entanglement renormalization to study 2D lattice models that are beyond the reach of quantum Monte Carlo techniques.

The present approach is based on the coarse-graining transformation of Fig. 1, which is applied to a kagome lattice $\mathcal{L}_0$ made of N sites. It maps blocks of 36 sites of $\mathcal{L}_0$ onto single sites of a coarser lattice $\mathcal{L}_1$ made of $N/36$ sites. A Hamiltonian H_0 defined on lattice $\mathcal{L}_0$ becomes an effective Hamiltonian H_1 on lattice $\mathcal{L}_1$. Analogously, the ground state $|\Psi_0\rangle$ of H_0 is transformed into the ground state $|\Psi_1\rangle$ of H_1. The transformation decomposes into three steps. First disentanglers u, unitary tensors that act on 9 sites, are applied across the corners of three neighboring blocks. Then disentanglers v are applied across the sides of two neighboring blocks; these tensors reduce ten sites (each described by a vector space $\mathbb{C}_2$ of dimension 2) into two effective sites (each described by a vector space $\mathbb{C}_{\tilde{\chi}}$ of dimension $\tilde{\chi}$). Finally isometries w map the remaining sites of each block into a single effective site of $\mathcal{L}_1$. Thus the tensors u, v, and w,

$$\begin{aligned} u^\dagger &: \mathbb{C}_2^{\otimes 9} \to \mathbb{C}_2^{\otimes 9}, & u^\dagger u &= I_{2^9}, \\ v^\dagger &: \mathbb{C}_2^{\otimes 10} \to \mathbb{C}_{\tilde{\chi}}^{\otimes 2}, & v^\dagger v &= I_{\tilde{\chi}^2}, \\ w^\dagger &: \mathbb{C}_2^{\otimes 6} \otimes \mathbb{C}_{\tilde{\chi}}^{\otimes 6} \to \mathbb{C}_\chi, & w^\dagger w &= I_\chi, \end{aligned} \tag{1}$$

transform the ground state $|\Psi_0\rangle$ of lattice $\mathcal{L}_0$ into the

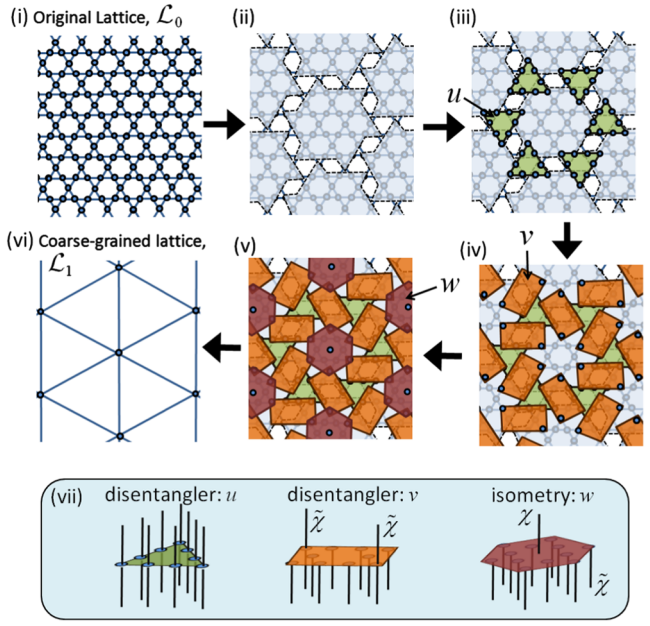

FIG. 1 (color online). Coarse-graining transformation that maps (i) a kagome lattice $\mathcal{L}_0$ of N sites into (vi) a coarser lattice $\mathcal{L}_1$ of $N/36$ sites. (ii) The lattice is first partitioned into blocks of 36 sites. (iii) Disentanglers u are applied across the corners of three blocks, followed by (iv) disentanglers v applied across the sides of two neighboring blocks. (v) Isometries w map blocks to an effective site of the coarse-grained lattice. (vii) Tensors u, v and w, have a varying number of incoming and outgoing indices according to Eq. (1).

ground state $|\Psi_1\rangle$ of lattice $\mathcal{L}_1$ through the sequence

$$|\Psi_0\rangle \xrightarrow{u} |\Psi_0'\rangle \xrightarrow{v} |\Psi_0''\rangle \xrightarrow{w} |\Psi_1\rangle. \tag{2}$$

The disentanglers u and v aim at removing short-range entanglement across the boundaries of the blocks; therefore states $|\Psi_0'\rangle$ and $|\Psi_0''\rangle$ possess decreasing amounts of short-range entanglement. If state $|\Psi_0\rangle$ only has short-range entanglement to begin with, then it is conceivable that the state $|\Psi_1\rangle$ has no entanglement left at all. For a finite lattice ($N = 144$) we consider a state $|\Psi_0\rangle$ that, after the coarse-graining transformation, gives rise to an entangled state $|\Psi_1\rangle$ on $N/36 = 4$ sites. For an infinite lattice we make instead an important assumption, namely, that $|\Psi_1\rangle$ is a product (nonentangled) state [this is equivalent to setting $\chi = 1$ in Eq. (1)]. How short ranged must the entanglement in $|\Psi_0\rangle$ be for this assumption to be valid? By reversing the transformation on a product state $|\Psi_1\rangle$, it can be seen that each site in $|\Psi_0\rangle$ is still entangled with at least 84 neighboring sites.

The disentanglers and isometries (u, v, w) were initialized randomly and then optimized so as to minimize the expectation value of the KLHM Hamiltonian

$$H_0 = J \sum_{\langle i,j \rangle} S_i \cdot S_j \tag{3}$$

by following the algorithms of Ref. [25], with cost $O(2^{12}\tilde{\chi}^6\chi^2)$ [26]. Specifically, for lattices with $N = 36$ and 144 sites, the resulting (one-site and four-site) Hamiltonian H_1 is diagonalized exactly. Instead, for $N = \infty$, we use the finite correlation range algorithm (Sec. V.D of Ref. [25]). All computations led to highly dimerized wave functions of the VBC type. In order to explain the results, consider the exact "honeycomb" VBC state, denoted $|h\text{-VBC}\rangle$, whose 36-site unit cell is shown in Fig. 2. Each unit cell contains two "perfect hexagons" (resonating bonds around a hexagon) and a "pinwheel." Three different types of strong bonds can be identified: those of the pinwheels (red), parallel bonds (green), and perfect hexagons (blue). The pinwheel and parallel bonds are singlets (energy per bond $= -0.75$) while the perfect hexagons are in the ground state of a periodic Heisenberg chain of 6 sites (energy per bond $= -0.4671$). The rest of the links have zero energy. We call a "honeycomb" VBC a state that has strong bonds according to the above pattern, even though the rest of bonds (weak bonds) need not have zero energy. The "honeycomb" VBC was originally proposed by Marston and Zeng [2] (see also [4,6,7]). Our simulations with $N = 144$ and $N = \infty$ produce a VBC of this type as the best MERA approximation to the ground state.

The energies obtained for an infinite lattice are shown in Table I. For each value of $\tilde{\chi}$ [see Eq. (1)], the MERA is an explicit wave function and therefore provides an upper bound to the exact ground state energy. Energies computed for the $N = 144$ lattice matched those of the infinite lattice to within 0.02% and have been omitted. Our $N = \infty$ energy

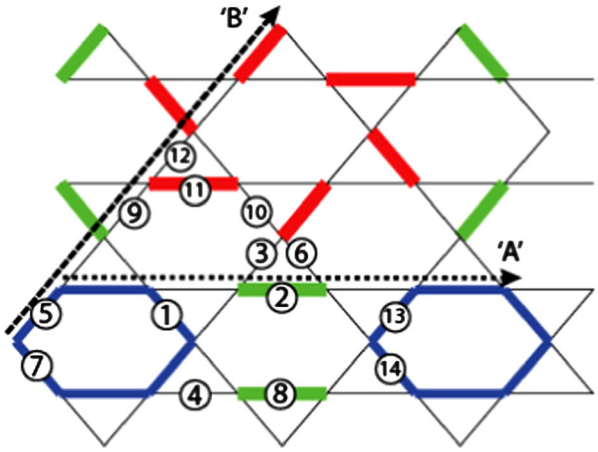

FIG. 2 (color online). The 36-site unit cell for the honeycomb VBC, strong bonds are drawn with thick lines. Three different types of strong bonds can be identified; the six bonds belonging to the pinwheels (red), six bonds belonging to each "perfect hexagon" (blue), and the parallel bonds between perfect hexagons (green). Dotted arrows indicate the axis where spin-spin correlators have been computed. Bond-bond correlators have been computed between the reference bond (1) and the other numbered bonds.

TABLE I. Ground state energies as a function of $\tilde{\chi}$.

$\tilde{\chi}$	$N = \infty$	$N = 36$ (Randomly initialized)	$N = 36$ ($\|h - \text{VBC}\rangle$ initialized)
2	−0.421 45	−0.421 64	−0.421 43
4	−0.429 52	−0.428 16	−0.427 15
8	−0.430 81	−0.431 99	−0.431 48
12	−0.431 14	−0.433 71	−0.432 98
16	−0.431 35	−0.434 90	−0.434 20
20	−0.431 62	−0.436 11	−0.435 41
26	−0.431 93		
32	−0.432 21		

is also compatible with the energy $E = -0.433 \pm 0.001$ for a VBC obtained with series expansion in Ref. [6], and is lower than that obtained in Ref. [16] with DMRG ($E = -0.431\,60$ for $N = 108$) and in Ref. [14] with fermionic mean-field theory and Gutzwiller projection ($E = -0.428\,63$ for $N = 432$). We further notice that, where finite size effects are still relevant, such as in the $N = 108$ case, they tend to decrease the ground state energy.

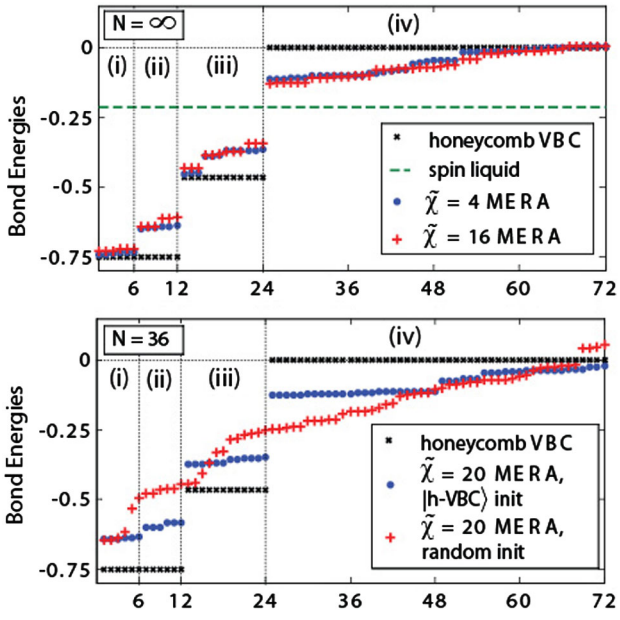

FIG. 3 (color online). (top) Bond energies for the 36-site unit cell of infinite MERA wave functions, for two different values of $\tilde{\chi}$, as compared to those of an exact honeycomb VBC, $|h\text{-VBC}\rangle$, and those of a spin liquid, which by definition has all equal strength bonds. The MERA wave functions clearly match the proposed honeycomb VBC; we identify (i) the six strong "pinwheel" bonds (red bonds), the six "parallel" bonds (green bonds), and (iii) the 12 "perfect hexagon" bonds (blue bonds). The (iv) remaining 48 bonds are the weak bonds of the unit cell. (bottom) Bond energies for the 36-site lattice. Here a randomly initialized MERA converges to a dimerized state that does not match the honeycomb VBC pattern, but gives lower overall energy than a honeycomb VBC initialized MERA of the same $\tilde{\chi}$.

Figure 3 shows the distribution of bond energies obtained for the $N = \infty$ lattice. With $\tilde{\chi} = 4$, one observes an energy increase per site over $|h\text{-VBC}\rangle$ of ≈ 0.08 in the parallel (green) bonds and also in some of the hexagon (blue) bonds, with the weak bonds having lower energy in return. As $\tilde{\chi}$ is increased, the energy of the "strong" bonds becomes slightly larger and that of the "weak" bonds continues to decrease. However, the dimerization clearly survives: the bond energies are not seen to converge to a uniform distribution as required for a SL.

Figure 4 shows spin-spin correlators evaluated along two different lattice axis A and B (cf. Fig. 2) for $N = \infty$. These correlators decay exponentially with well-defined "plateaus," where the correlation is the same with both spins of a strong bond. Correlations along the line joining a perfect hexagon and a pinwheel are seen to decay faster than along the line joining two perfect hexagons, consistent with the observation from Fig. 3 that the pinwheel bonds remain almost exact singlets even for high values of $\tilde{\chi}$. Table II shows bond-bond connected and disconnected correlators, $C_{1,\alpha}$ and $D_{1,\alpha}$,

$$C_{1,\alpha} \equiv \langle (\vec{S}\cdot\vec{S})_1 (\vec{S}\cdot\vec{S})_\alpha \rangle, \tag{4}$$

$$D_{1,\alpha} \equiv C_{1,\alpha} - \langle (\vec{S}\cdot\vec{S})_1 \rangle \langle (\vec{S}\cdot\vec{S})_\alpha \rangle, \tag{5}$$

between a reference bond "1" and a surrounding bond $\alpha = 1, \ldots, 14$ (cf. Fig. 2). While disconnected correlators decay exponentially with distance, some connected correlators remain significant at arbitrary distances, demonstrating the long-range order of the VBC state.

Let us discuss the results for a lattice with $N = 36$ sites. When initialized with random tensors, the MERA pro-

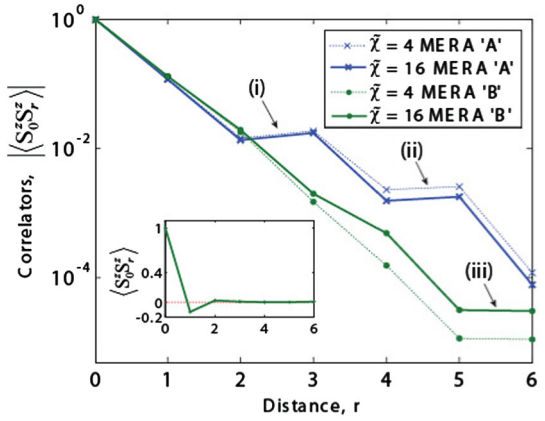

FIG. 4 (color online). Spin-spin correlators along arrows "A" and "B" of Fig. 2 for infinite lattice MERA of $\tilde{\chi} = 4$ and $\tilde{\chi} = 16$. Although along both lattice directions considered the correlators decay exponentially, the decay along arrow "A" (a line joining two perfect hexagons) is seen to be slower than along arrow "B" (a line joining perfect hexagon to pinwheel). The plateaus marked (i), (ii), and (iii) show the correlation is the same with both spins of a strong bond.

TABLE II. Bond-bond correlators for $\tilde{\chi} = 16$ ($N = \infty$).

Bond	$C_{1,\alpha}$	$D_{1,\alpha}$	$\langle(\vec{S}\cdot\vec{S})_\alpha\rangle$
1	0.386 39	0.228 15	−0.397 80
2	0.294 90	0.034 96	−0.653 42
3	0.004 22	−0.001 15	−0.013 49
4	0.095 03	0.046 44	−0.122 11
5	0.224 88	0.066 09	−0.399 18
6	−0.006 09	−0.014 26	−0.020 54
7	−0.103 72	−0.033 76	−0.345 61
8	0.260 83	0.012 52	−0.624 21
9	0.003 36	0.003 68	0.000 82
10	−0.000 01	−0.000 17	−0.000 42
11	0.291 13	0.001 96	−0.726 93
12	0.000 90	−0.000 36	−0.003 21
13	0.166 32	0.000 26	−0.417 44
14	0.156 74	−0.000 37	−0.394 96

duced VBC type configurations which typically did not match the honeycomb VBC, although simulations initialized in the state $|h\text{-VBC}\rangle$ retained the honeycomb VBC pattern (see Fig. 3). Here the randomly initialized VBC produced a lower energy (0.5% above the exact diagonalization result $E = -0.438\,377$ of [9]) than the honeycomb VBC type solution for an equivalent value of $\tilde{\chi}$ (cf. Table I). These results strongly suggest that finite size effects in the $N = 36$ site lattice lead to a significant departure from the physics of the infinite system.

To summarize, we have used entanglement renormalization techniques to obtain new numerical evidence indicating that the ground state of the KLHM is of the honeycomb VBC type. In order to assess the robustness of this result, we briefly discuss some of the limitations of the present approach.

First, the coarse-graining transformation of Fig. 1, which maps 36 sites into one site, was designed to ensure compatibility with the 36-site unit cell of honeycomb VBC type solutions. While our approach did not preclude solutions with a smaller, compatible unit cell (such as a 12-site unit cell or a fully translation invariant solution), we cannot rule out the possibility that a state with an incompatible unit cell might have a lower energy.

Second, the infinite lattice was investigated by restricting the range of entanglement in the ansatz to blocks of 84 spins, imposed through an unentangled state $|\Psi_1\rangle$ in Eq. (2). This restriction was only implemented after preliminary simulations with $\tilde{\chi} = 12$ had produced identical energies irrespectively of whether $|\Psi_1\rangle$ was allowed to be entangled. However, it could still be that entanglement in $|\Psi_1\rangle$ would make a big difference for larger values of $\tilde{\chi}$. We find this scenario quite unlikely, but could not test it due to computational limitations.

Finally, the MERA is an essentially unbiased method provided that the candidates to be the ground state of the system have all a relatively small amount of entanglement. But when deciding between a VBC (which mostly has short-range entanglement) and, e.g., the algebraic SL of Refs. [14,15] (significantly more entangled at all length scales), it might well be that the MERA is biased toward the low entanglement solution. Therefore our results do not conclusively exclude a SL ground state. We emphasize, however, that the ground state energies obtained with the MERA are lower than the SL energies of Refs. [14–16].

We thank P. Lee, R. Singh, X.-G. Wen, and S. White for valuable conversations. Support from the Australian Research Council (APA, FF0668731, DP0878830) is acknowledged.

[1] For a review, see C. Lhuillier, arXiv:cond-mat/0502464v1.
[2] J. B. Marston and C. Zeng, J. Appl. Phys. **69**, 5962 (1991).
[3] A. V. Syromyatnikov and S. V. Maleyev, Phys. Rev. B **66**, 132408 (2002).
[4] P. Nikolic and T. Senthil, Phys. Rev. B **68**, 214415 (2003).
[5] R. Budnik and A. Auerbach, Phys. Rev. Lett. **93**, 187205 (2004).
[6] R. R. P. Singh and D. A. Huse, Phys. Rev. B **76**, 180407(R) (2007).
[7] R. R. P. Singh and D. A. Huse, Phys. Rev. B **77**, 144415 (2008).
[8] S. Sachdev, Phys. Rev. B **45**, 12 377 (1992).
[9] P. W. Leung and V. Elser, Phys. Rev. B **47**, 5459 (1993).
[10] F. Wang and A. Vishwanath, Phys. Rev. B **74**, 174423 (2006).
[11] F. Mila, Phys. Rev. Lett. **81**, 2356 (1998).
[12] M. B. Hastings, Phys. Rev. B **63**, 014413 (2000).
[13] M. Hermele, T. Senthil, and M. P. A. Fisher, Phys. Rev. B **72**, 104404 (2005).
[14] Y. Ran, M. Hermele, P. A. Lee, and X. -G. Wen, Phys. Rev. Lett. **98**, 117205 (2007).
[15] M. Hermele *et al.*, Phys. Rev. B **77**, 224413 (2008).
[16] H. C. Jiang, Z. Y. Weng, and D. N. Sheng, Phys. Rev. Lett. **101**, 117203 (2008).
[17] M. P. Shores *et al.*, J. Am. Chem. Soc. **127**, 13 462 (2005).
[18] A. M. Läuchli and C. Lhuillier, arXiv:0901.1065v1.
[19] G. Vidal, Phys. Rev. Lett. **99**, 220405 (2007).
[20] G. Vidal, Phys. Rev. Lett. **101**, 110501 (2008).
[21] G. Evenbly and G. Vidal, arXiv:0710.0692v2 [Phys. Rev. B (to be published)].
[22] G. Evenbly and G. Vidal, New J. Phys. **12**, 025007 (2010).
[23] L. Cincio, J. Dziarmaga, and M. M. Rams, Phys. Rev. Lett. **100**, 240603 (2008).
[24] G. Evenbly and G. Vidal, Phys. Rev. Lett. **102**, 180406 (2009).
[25] G. Evenbly and G. Vidal, Phys. Rev. B **79**, 144108 (2009).
[26] The computational cost of simulations can be significantly reduced by incorporating symmetries of the system into the MERA tensor network [27]. In this work, a $U(1)$ symmetry is incorporated into the MERA to allow large $\tilde{\chi}$ simulations that would otherwise be unaffordable.
[27] S. Singh, R. N. C. Pfeifer, and G. Vidal, arXiv:0907.2994v1.